JOURNAL OF MATERIALS SCIENCE 27 (1992) 5008–5014

# Oxidation behaviour of β-sialon fabricated from α-$Si_3N_4$ and aluminium iso-propoxide

KAZUSHI KISHI, SEIKI UMEBAYASHI
*Government Industrial Research Institute, Kyushu Shuku-machi, Tosu-shi, Saga 841, Japan*

β-sialon with $z = 0.5$ was fabricated by hot pressing of a spray-dried mixture of α-$Si_3N_4$ and aluminium iso-propoxide solution. The oxidation behaviour of this β-sialon was investigated, comparing it with commercial β-sialon containing $Y_2O_3$ as a sintering aid. Oxidation tests were carried out at 1200 and 1400 °C for 25 to 200 h in air. The oxide layer of aluminium iso-propoxide-derived β-sialon was thin, dense, smooth and homogeneous without bubbles and cracks. The strength after oxidation at 1400 °C for 200 h was about 800 MN m$^{-2}$, almost the same value as before oxidation. The oxide layer of $Y_2O_3$-doped β-sialon was thick and inhomogeneous, containing many bubbles, cracks and grown needle-like crystallites ($Y_2Si_2O_7$). The strength after oxidation at 1200 °C for 200 h fell to $\frac{1}{2}$ (440 MN m$^{-2}$) because of pit formation in the oxide layer, and at 1400 °C for 200 h fell to $\frac{1}{4}$ (200 MN m$^{-2}$) because of severe swelling and flaking of the oxide layer. The high oxidation resistance of aluminium iso-propoxide derived β-sialon was mainly due to its homogeneous microstructure and freedom from foreign constituents such as $Y_2O_3$.

## 1. Introduction

β-sialon ($Si_{6-z}Al_zO_zN_{8-z}$) is of interest for application in ceramic components for engines and other high-temperature engineering, because of its excellent properties such as high-temperature strength and high oxidation resistance [1].

Commonly, β-sialon is fabricated from a powder mixture of $Si_3N_4$, $Al_2O_3$ and AlN [2–8]. However, the strength of this β-sialon is still low compared with $Si_3N_4$ sintered bodies [9–12]. The authors have reported that β-sialon fabricated from $Si_3N_4$ powder and aluminium iso-propoxide solution has a homogeneous microstructure and the strength of it was much improved [13–16] compared with conventional β-sialon fabricated from a powder mixture.

On the other hand, high-strength $Y_2O_3$-doped β-sialon is developed and commercially produced [17–20]. The oxidation behaviour of this β-sialon should be different from that of β-sialon without $Y_2O_3$, because $Y_2O_3$-doped β-sialon consists of β-sialon grains and a relatively larger amount of grain-boundary phase where $Y_2O_3$ and $Al_2O_3$ is concentrated.

The oxidation behaviour of aluminium iso-propoxide-derived β-sialon compared with commercial β-sialon sintered with $Y_2O_3$ is described.

## 2. Experimental procedure

The fabrication procedure of β-sialon from α-$Si_3N_4$ and aluminium iso-propoxide was described in previous papers [14–16]. The commercial β-sialon containing $Y_2O_3$ as a sintering aid was purchased from Hitachi Metal Co. Ltd (HCN-10).

Specimens 3 mm × 3 mm × 30 mm for oxidation tests were prepared by grinding with a No. 600 diamond wheel and chamfering with No. 800 SiC abrasive paper. Oxidation tests were carried out at 1200 and 1400 °C for 25, 50, 100 and 200 h in air. Fig. 1 showed a schematic sketch of the specimens during oxidation.

Bending strength after oxidation was measured at room temperature using a three-point loading device with a span of 20 mm and a crosshead speed of 0.5 mm min$^{-1}$.

Table I showed the properties of the samples, hereinafter designated as samples A and B.

## 3. Results and discussion

### 3.1. Oxidation weight gain and observation of oxide layer

The crystalline phases in the oxide layer, identified by X-ray diffraction (XRD), were cristobalite in sample A and yttrium silicate ($Y_2Si_2O_7$) and cristobalite in sample B.

Fig. 2 shows the oxidation weight gain of samples as a function of oxidation time. The oxidation weight gain increased with increasing oxidation time and temperature in both samples. However, sample A showed a remarkably lower oxidation weight gain than sample B at both temperatures.

Fig. 3 shows optical micrographs of oxidized surfaces of sample A and Fig. 4 shows SEM photographs of fractured surfaces of the oxide layer. The thickness of the oxide layer increased with increasing oxidation temperature and time. The thickness of the oxide layer was about 8 μm even after oxidation at 1400 °C for



0022–2461 

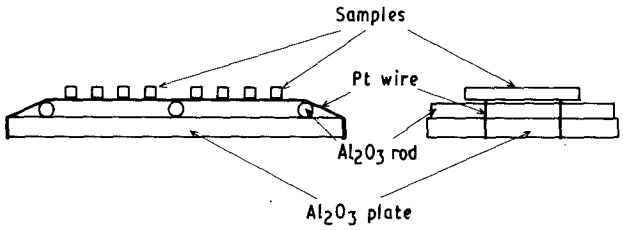


*Figure 1* Sketch of the samples during oxidation.

TABLE I Properties of samples

| Sample | A | B[a] |
|---|---|---|
| Starting materials | $Si_3N_4$ + Al(Oi-Pr)$_3$ | |
| Additive | – | $Y_2O_3$ |
| Phase composition | β + O′ | β |
| Density (g cm$^{-3}$) | 3.14 | 3.26 |
| Bending strength (MN m$^{-2}$) | 850 | 880 |
| Vickers hardness (GN m$^{-2}$) | 16.0 | 15.5 |
| $K_{Ic}$ (MN m$^{-3/2}$) | 3.3 | 6.0 |

[a] Catalogue material, Hitachi Metal Co. Ltd.

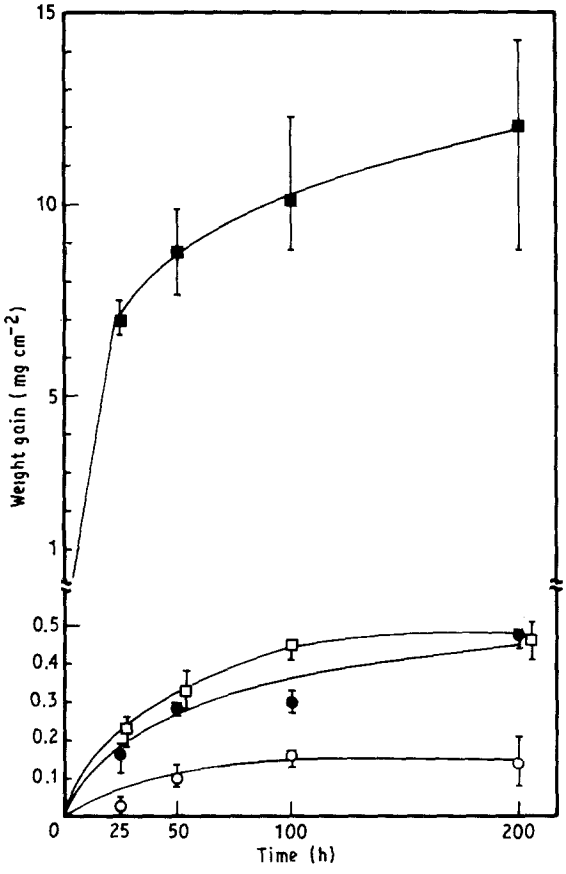


*Figure 2* Weight change versus oxidation time at 1200 and 1400 °C in air. Sample A: (○) 1200 °C, (●) 1400 °C. Sample B: (□) 1200 °C, (■) 1400 °C.

200 h, and the oxide layer appeared smooth and homogeneous without bubbles and cracks.

Previous studies on the oxidation behaviour of β-sialon indicated that the oxidation proceeded via diffusion of $O_2$ (O, $O^{2-}$) and produced $N_2$ and/or NO gas removed as bubbles in the oxide layer [21–24]. The oxidation reaction of β-sialon can be summarized by the equation [22]

$$4Si_5AlON_7 + 21O_2(g) \rightarrow 20SiO_2 \cdot 2Al_2O_3 + 14N_2(g)\uparrow \quad (1)$$

In sample A, formation of bubbles by removal of $N_2$ and/or NO as gas did not occur either in the oxide layer or on the oxide–substrate interface as shown in Figs 3 and 4. This difference in oxidation behaviour between aluminium iso-propoxide-derived β-sialon and conventional β-sialon from a powder mixture could be explained as given below.

β-sialon fabricated from a powder mixture includes many inhomogeneous regions where liquid phase is concentrated, and/or clustered large grains which originate from inhomogeneous mixing and dispersion of the starting powders [4, 5, 7, 8, 13, 25]. An optical micrograph of the fractured surface of β-sialon fabricated from a powder mixture of $Si_3N_4$ and $Al_2O_3$ [16] after oxidation at 1400 °C for 200 h is shown in Fig. 5. A bubble formed from an inhomogeneous region (a black spot) became a fracture origin as indicated by an arrow in Fig. 5. These black spots are assumed to be regions where an oxygen-rich liquid phase had been concentrated [13]. Thus, the liquid phase accelerated the oxidation reaction and resulted in bubble formation. If the microstructure of the sample was homogeneous, the oxidation reaction should proceed more homogeneously and slowly, and then the bubbling would not occur. This could be the reason why sample A showed a thin, homogeneous and smooth oxide layer without bubbling.

Optical micrographs of the oxidized surface of sample B are shown in Fig. 6 and SEM micrographs of the fractured surface are shown in Fig. 7. Sample B shows a different appearance compared with sample A. Thus, the oxide layer consists of many bubbles, grown needle-like crystallites and cracks. The oxidation mechanism of β-sialon sintered with $Y_2O_3$ has been reported [22] and it was indicated that Y ions migrated from the grain-boundary phase to the surface oxide layer and crystallized as an yttrium silicate such as $Y_2Si_2O_7$.

Optical micrographs of the surface of $Y_2O_3$- and $Al_2O_3$-doped $Si_3N_4$ oxidized at 1200 °C for 100 h are shown in Fig. 8. The appearance of the oxide layer is very similar to that of sample B and this suggests that the oxidation mechanisms of the two sintered bodies were also similar. The oxidation mechanism of $Y_2O_3$- and $Al_2O_3$-doped $Si_3N_4$ has been reported and it was indicated that Y ions migrated from the grain-boundary phase to the oxide layer and crystallized [26, 27] in the same way as in $Y_2O_3$-doped β-sialon. From the viewpoint of $Si_3N_4$ sintered bodies, the formation of a relatively dense oxide layer containing yttrium silicate was better than the porous oxide layer which appeared in MgO-doped $Si_3N_4$ [28, 29]. However, this concentration of yttrium resulted in a more porous oxide layer and a decrease of the oxidation resistance compared with β-sialon without $Y_2O_3$ [22] and CVD $Si_3N_4$ [27]. Ultimately, to have an yttrium-rich grain-boundary phase should bring a decrease of oxidation resistance.

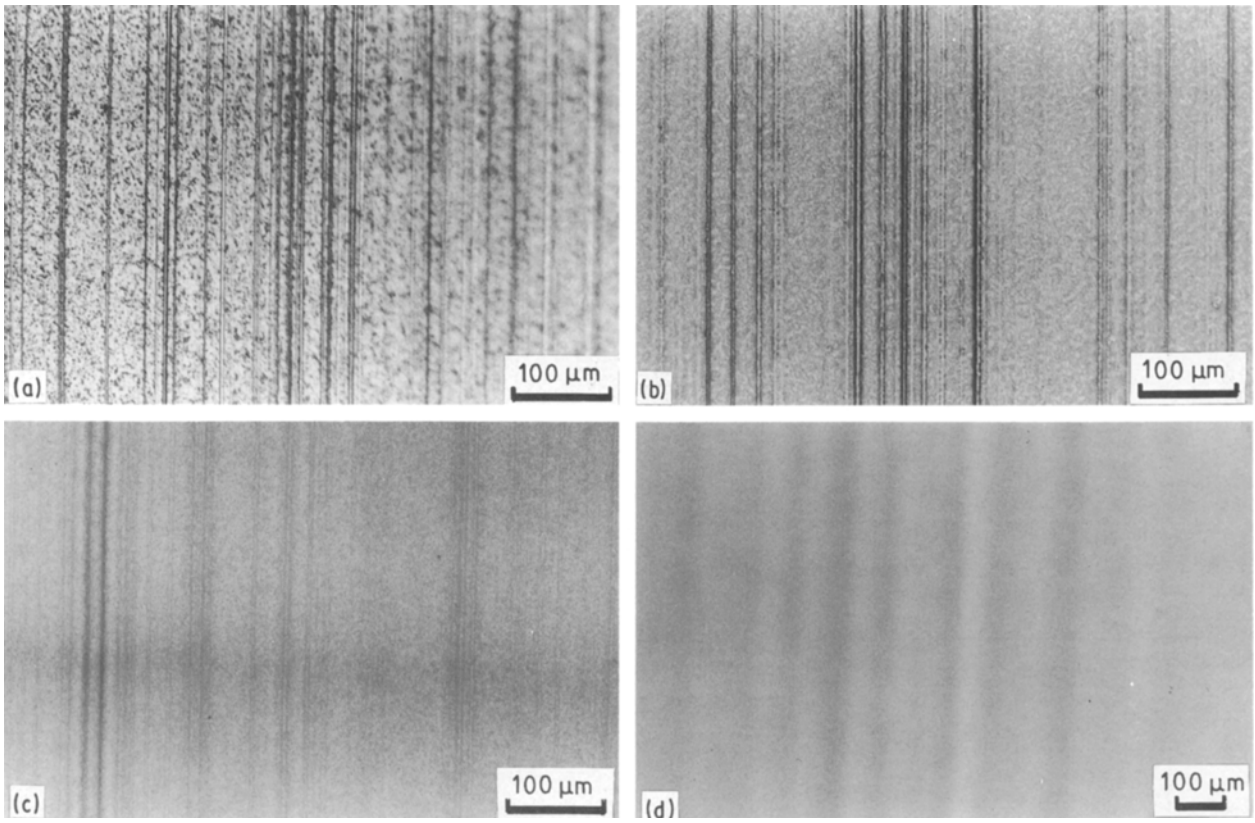


*Figure 3* Optical micrographs of oxidized surfaces of sample A: (a) as ground; (b) 1200 °C, 50 h; (c) 1200 °C, 200 h; (d) 1400 °C, 25 h.

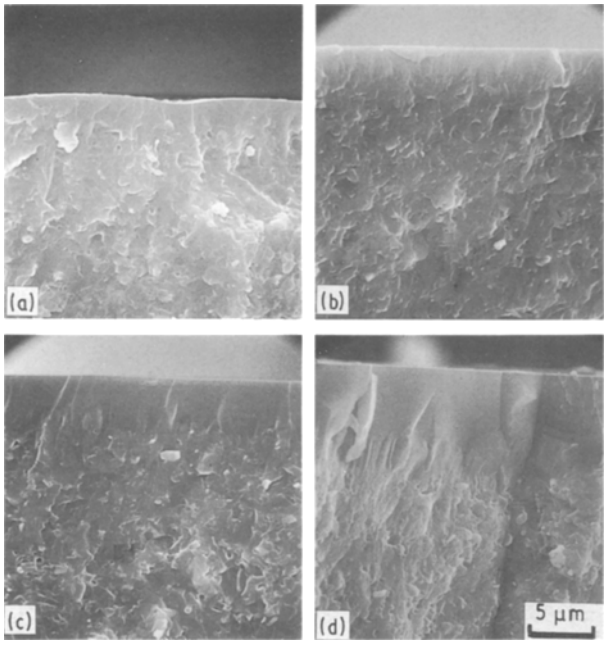


*Figure 4* SEM photographs of fractured surface of sample A after oxidation: (a) 1200 °C, 25 h; (b) 1200 °C, 200 h; (c) 1400 °C, 25 h; (d) 1400 °C, 200 h.

From these results, it could be concluded that the high oxidation resistance of sample A was mainly due to its homogeneous microstructure and freedom from foreign constituents such as $Y_2O_3$.

## 3.2. Change of bending strength with oxidation

Fig. 9 shows the change of the bending strength of

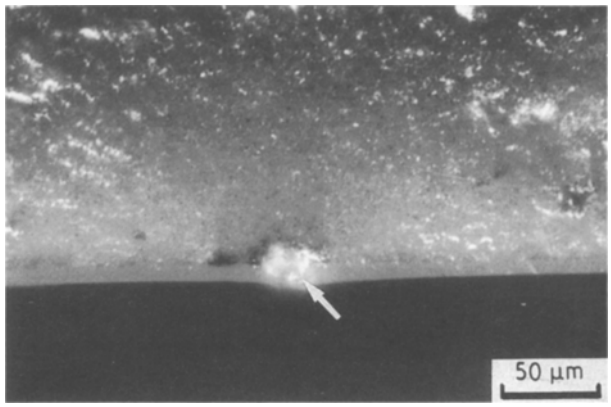


*Figure 5* Optical micrographs of β-sialon fabricated from powder mixture of $Si_3N_4$ and $Al_2O_3$ after oxidation at 1400 °C for 200 h; the arrow indicates a bubble formed from a black spot.

samples as a function of oxidation time. The strength of sample A oxidized for 25 h was increased to 1400 MN m$^{-2}$, but subsequently it decreased and after 200 h it became about 800 MN m$^{-2}$ at both temperatures; after oxidation at 1400 °C for 400 h it was 780 MN m$^{-2}$, not so much decreased from the original level.

Optical micrographs of fractured surfaces of sample A are shown in Fig. 10. All the fracture origins of unoxidized specimens were surface grinding flaws and those of oxidized specimens were the oxide–substrate interface as shown in Fig. 10b, c and d.

The increase of strength in samples oxidized for 25 h is assumed to be due to the blunting of crack tips derived from grinding flaws, and the coating of surface flaws with an oxide layer [15].

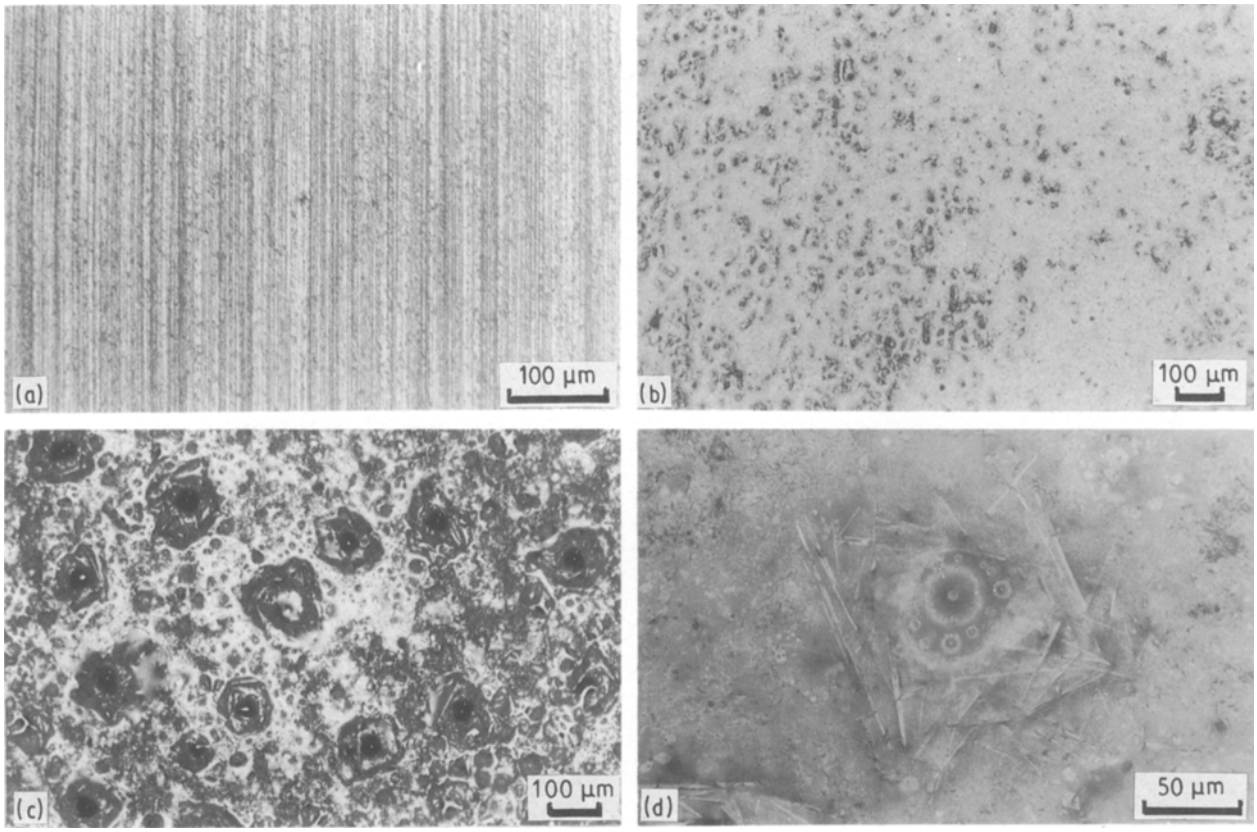


*Figure 6* Optical micrographs of oxidized surfaces of sample B: (a) as ground; (b) 1200 °C, 25 h; (c,d) 1200 °C, 50 h.

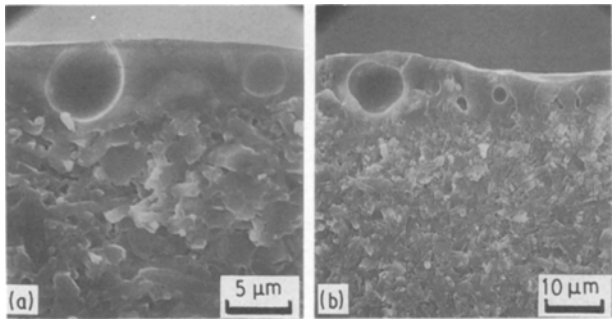


*Figure 7* SEM photographs of fractured surface of sample B after oxidation: (a) 1200 °C, 25 h; (b) 1200 °C, 200 h.

The bending strength of specimens of sample A is shown as a function of the oxidation weight gain in Fig. 11. In general, the strength was decreased with increasing weight gain. However, many specimens with a higher weight gain showed a higher strength than those with a lower weight gain. The lowest strength is assumed to be confined to the original strength level of as-ground specimens.

On the basis of an infrared reflection spectroscopic (IRRS) study of the oxide layer of β-sialon, Takase [30] has described how the surface of the oxide layer of β-sialon without additives changes from a crystalline one (cristobalite) to a glassy one by oxidation for more than 30 h due to the migration of Al and other metallic impurities. This suggests that the oxide layer consists of two separate layers, the outer layer being composed of a glassy phase and the inner one consisting of cristobalite. This type of separation of oxide layers has been also indicated by Lewis and Barnard [22].

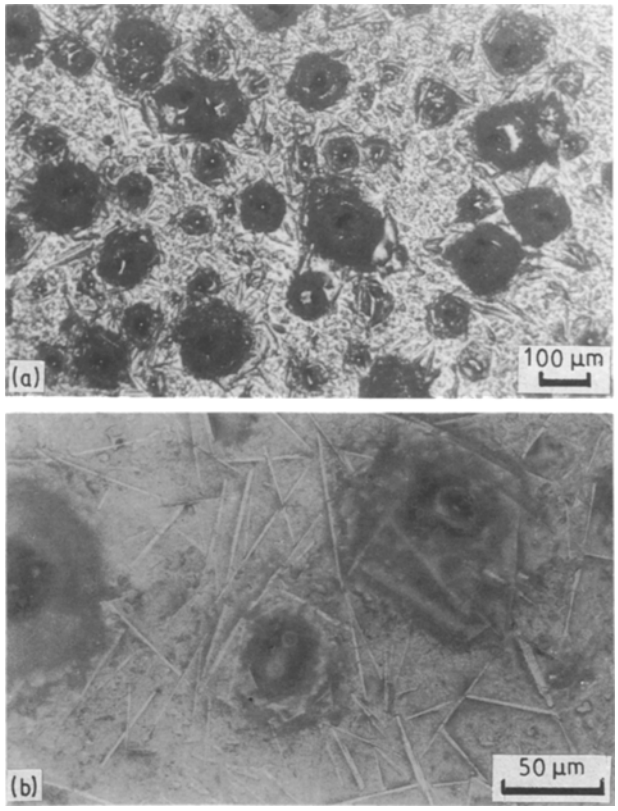


*Figure 8* Optical micrographs of oxidized surface of $Si_3N_4$ sintered with $Y_2O_3$ and $Al_2O_3$ (1200 °C, 100 h).

Fig. 12 shows an SEM photograph of an obliquely fractured oxide layer of sample A oxidized at 1400 °C for 200 h. There can be observed two layers as indicated in Fig. 12 as (A) and (B). They are assumed to

correspond to the two oxide layers which Lewis and Barnard [22] and Takase [30] have described. It can be observed that layer (A) and the substrate were fractured at the same angle, but layer (B) was fractured perpendicular to the substrate. This appearance of the fractured surface suggests the existence of residual stress on the oxide–substrate interface.

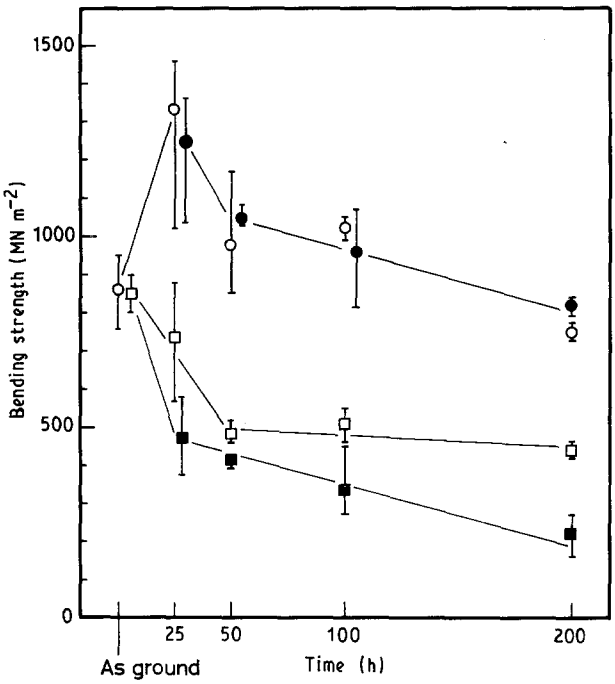


*Figure 9* Bending strength versus oxidation time at 1200 and 1400 °C in air. Sample A: (○) 1200 °C, (●) 1400 °C. Sample B: (□) 1200 °C, (■) 1400 °C.

From these results, the reason for the strength degradation of sample A oxidized for more than 50 h is considered to be as follows. As the $K_{Ic}$ of sample A is low, the surface grinding flaws should be deeper than the thickness of the oxide layer as shown in Fig. 10a. The cracks derived from grinding flaws should be filled with oxidation products, but they keep their original size even after oxidation [15, 31]. So, it is considered that deep grinding flaws of sample A which could be fracture origins are still present in the substrate even after oxidation. The stress occurring on the oxide–substrate interface is assumed to increase rapidly when the oxidation time becomes around 50 h, by the separation of oxide layers which Takase [30] has described. This increase of the stress is assumed to influence the oxidized grinding flaws mentioned above and to bring about the decrease of strength.

The strength of sample B oxidized at 1200 °C for 50 h decreased to 500 MN m$^{-2}$ and it was almost unchanged up to 200 h, but the strength of material oxidized at 1400 °C decreased with increasing oxidation time and became about 200 MN m$^{-2}$ ($\frac{1}{4}$ of the original strength) after 200 h as shown in Fig. 9.

Fig. 13 shows optical micrographs of fractured surfaces of sample B. The fracture origins in all specimens of sample B oxidized at 1200 °C for more than 50 h were large bubbles formed in the oxide layer (Fig. 13a and b). The specimens oxidized at 1400 °C showed significant swelling and flaking of the oxide layer as shown in Fig. 13c and d. Due to this roughening of the surface, the strength was continuously decreased.

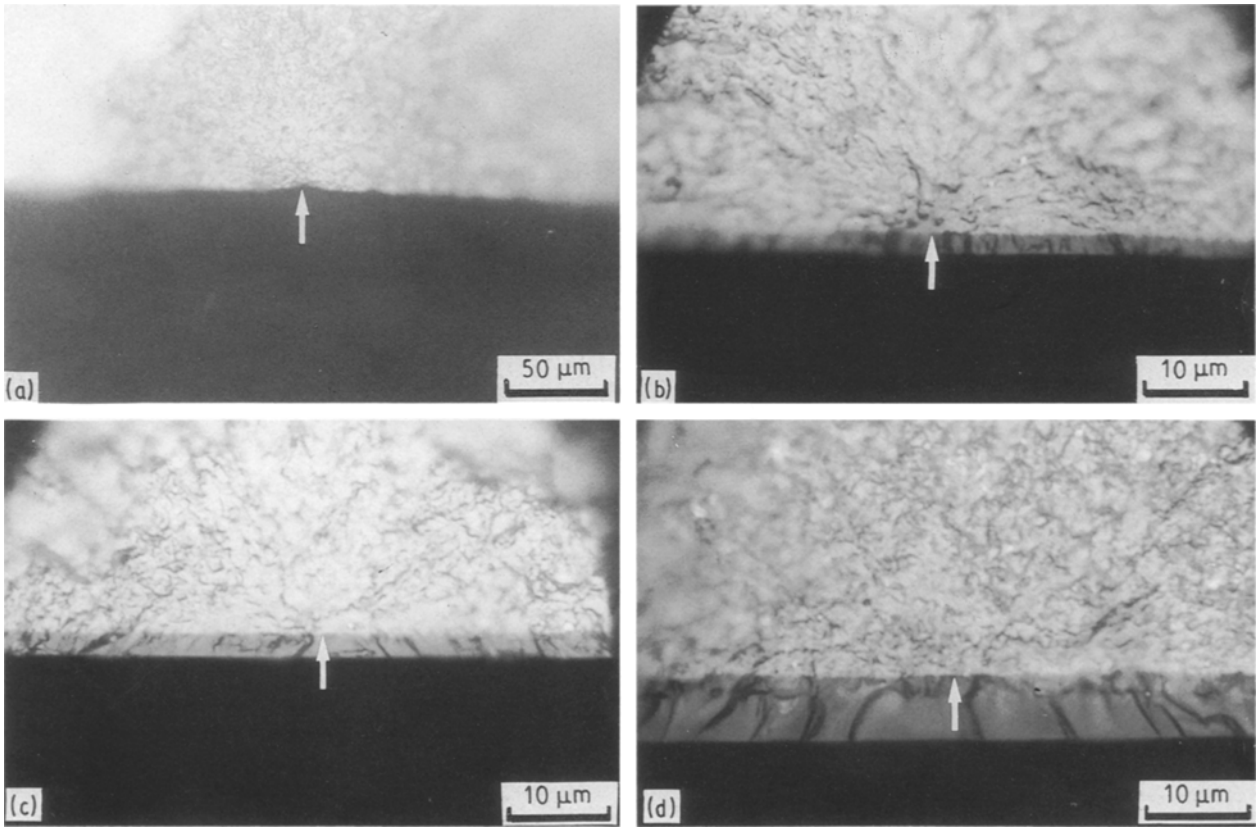


*Figure 10* Optical micrographs of fracture origins of sample A (arrows indicate fracture origins): (a) as ground (949 MN m$^{-2}$); (b) 1200 °C, 200 h (756 MN m$^{-2}$); (c) 1400 °C, 25 h (1375 MN m$^{-2}$); (d) 1400 °C, 200 h (829 MN m$^{-2}$).

The strength degradation of sample B oxidized at 1200 °C can be explained by this bubbling in the oxide layer. The bending strength of each specimens of sample B is shown as a function of the oxidation weight gain in Fig. 14. The strength was distinguishable as following three stages according to changes in the oxidation weight gain. In the first stage, with a small weight gain of less than 0.2 mg cm$^{-2}$, the strength showed almost the same values as that before oxidation, where the oxide layer was smooth and homogeneous as shown in Fig. 6b. For $Si_3N_4$ sintered bodies, it has been reported that in the early stage of oxidation the strength can be improved due to the healing and blunting of cracks derived from surface machining flaws [32, 33]. The first stage of sample B is considered to correspond to this early stage of oxidation. In the second stage, with a weight gain of about 0.25 mg cm$^{-2}$, the strength decreased rapidly due to the formation and increasing size of bubbles as fracture origins as shown in Fig. 13a. In the third stage,

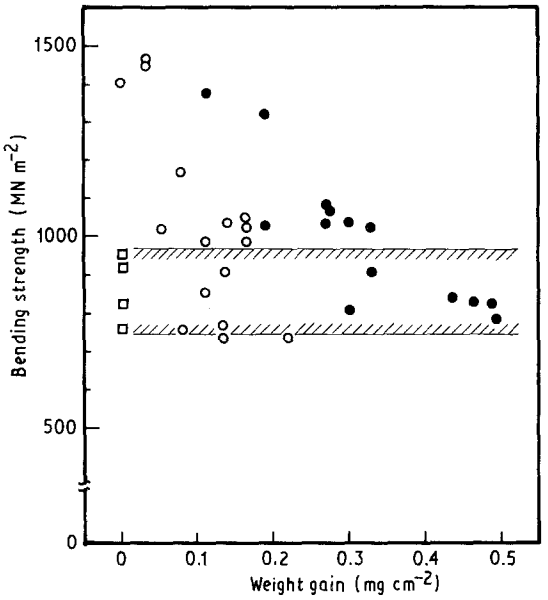


*Figure 11* Bending strength of sample A versus oxidation weight gain: (□) as ground; (○) 1200 °C, 25–200 h; (●) 1400 °C, 25–200 h.

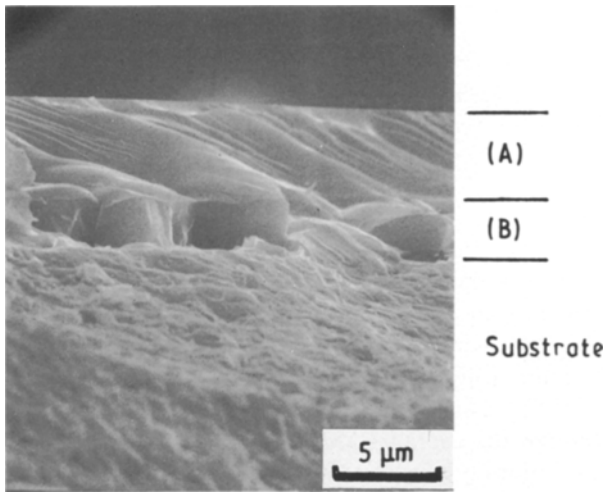


*Figure 12* SEM photograph of obliquely fractured oxide layer of sample A, indicating two oxide layers (A) and (B) (oxidized at 1400 °C for 200 h).

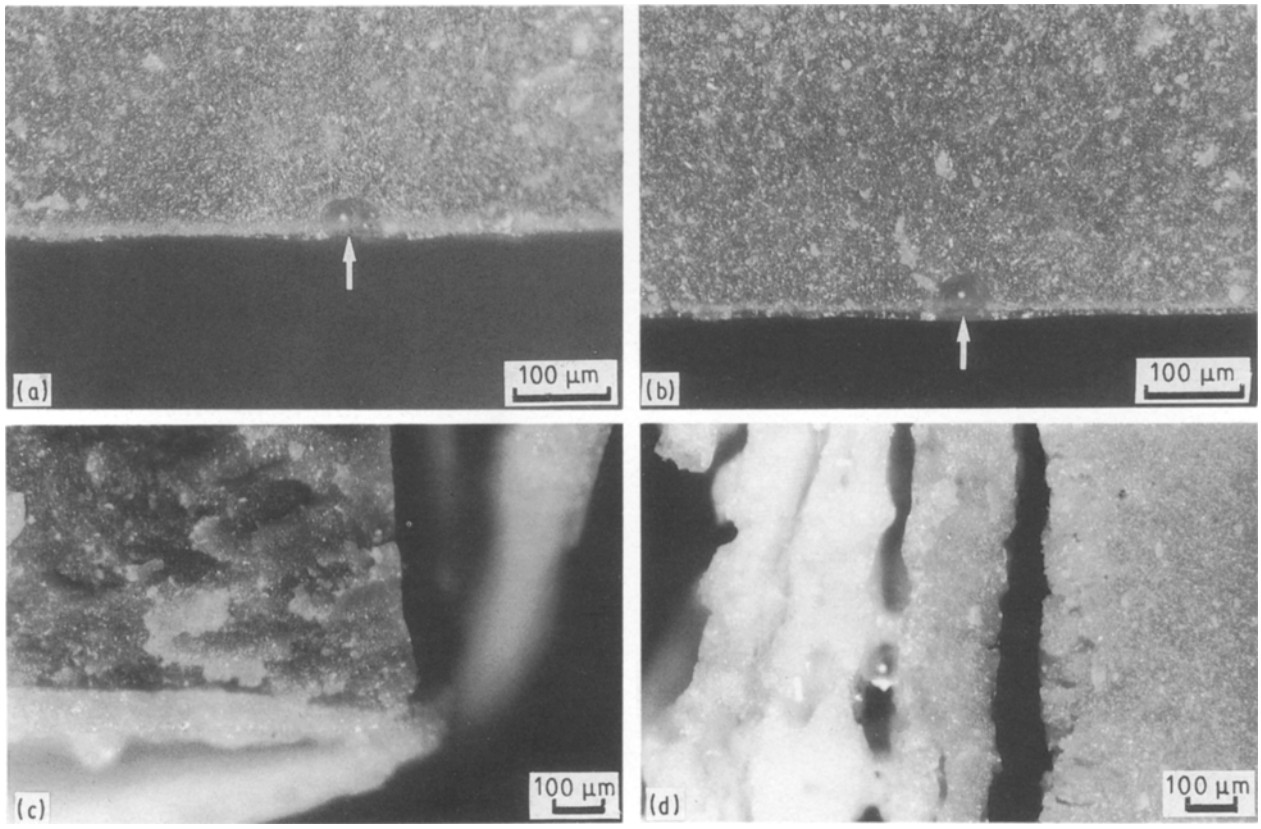


*Figure 13* Optical micrographs of fracture origins of sample B (arrows indicate fracture origins; in the specimens oxidized at 1400 °C the fracture origins could not be detected). (a) 1200 °C, 50 h (464 MN m$^{-2}$); (b) 1200 °C, 200 h (445 MN m$^{-2}$); (c) 1400 °C 25 h (413 MN m$^{-2}$); (d) 1400 °C, 200 h (200 MN m$^{-2}$).

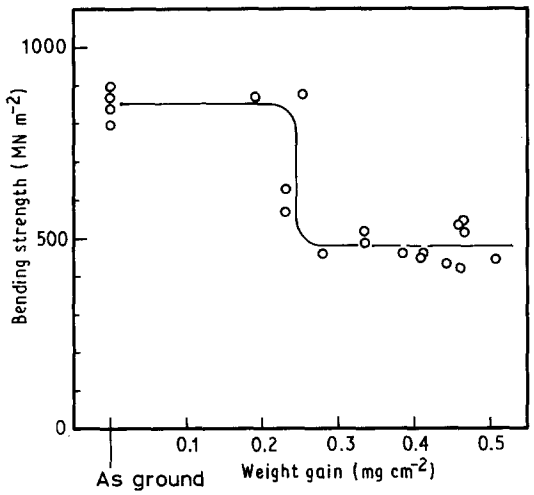


*Figure 14* Bending strength of sample B versus oxidation weight gain at 1200 °C, 25–200 h.

with a weight gain of more than 0.3 mg m$^{-2}$, the strength was almost constant even though the weight gain was increased. In this stage, the size of bubbles as fracture origins was almost constant as shown in Fig. 13b; hence the strength did not decrease, even though the average thickness of the oxide layer (the oxidation weight gain) was increased.

## 4. Conclusions

β-sialon with $z = 0.5$ was fabricated by hot pressing of a spray-dried mixture of α-$Si_3N_4$ and aluminium iso-propoxide solution. The oxidation behaviour of this β-sialon was investigated, comparing it with commercial β-sialon containing $Y_2O_3$ as a sintering aid. Oxidation tests were carried on at 1200 and 1400 °C for 25 to 200 h in air. The oxide layer of β-sialon derived from aluminium iso-propoxide was thin, dense, smooth and homogeneous without bubbles and cracks. The strength after oxidation at 1400 °C for 200 h was about 800 MN m$^{-2}$, almost the same value as before oxidation. The oxide layer of $Y_2O_3$-doped β-sialon was thick and inhomogeneous, containing many bubbles, cracks and grown needle-like crystallites ($Y_2Si_2O_7$). The strength after oxidation at 1200 °C for 200 h fell to $\frac{1}{2}$ (440 MN m$^{-2}$) because of pit formation in the oxide layer, and at 1400 °C for 200 h fell to $\frac{1}{4}$ (200 MN m$^{-2}$) because of severe swelling and flaking of the oxide layer. The high oxidation resistance of aluminium iso-propoxide derived β-sialon was mainly due to its homogeneous microstructure and freedom from foreign constituents such as $Y_2O_3$.

## References


1. K. H. JACK, *J. Mater. Sci.* **11** (1976) 1135.
2. M. MITOMO, N. KURAMOTO, M. TSUTSUMI and H. SUZUKI, *Yogyo-kyokai-shi* **86** (1978) 526.
3. R. R. WILLS, R. W. STEWART and J. M. WIMMER, *J. Amer. Ceram. Soc.* **60** (1977) 64.
4. M. MITOMO, Y. HASEGAWA, Y. BANDO, A. WATANABE and H. SUZUKI, *Yogyo-kyokai-shi* **88** (1980) 298.
5. M. MITOMO, N. KURAMOTO, Y. INOMATA and M. TSUTSUMI, *ibid.* **88** (1980) 489.
6. M. N. RAHAMAN, F. L. RELEY and R. J. BROOK, *J. Mater. Sci.* **16** (1981) 660.
7. S. UMEBAYASHI, K. KISHI, K. KOBAYASHI, K. MIYAZAKI and T. OOYAMA, *Yogyo-kyokai-shi* **90** (1982) 615.
8. S. UMEBAYASHI, K. KISHI, E. TANI and K. KOBAYASHI, *ibid.* **92** (1984) 35.
9. F. F. LANGE, *J. Amer. Ceram. Soc.* **57** (1974) 84.
10. A. TSUGE and K. NISHIDA, *Amer. Ceram. Soc. Bull.* **57** (1978) 424.
11. A. GIACHELLO, P. C. MARTINENGO, G. TOMMASINI and P. POPPER, *ibid.* **59** (1980) 1212.
12. R. K. GOVILA, *J. Mater. Sci.* **23** (1988) 1141.
13. K. KISHI, S. UMEBAYASHI, E. TANI and K. KOBAYASHI, *Yogyo-kyokai-shi* **93** (1985) 629.
14. *Idem., ibid.* **94** (1986) 179.
15. *Idem., ibid.* **95** (1987) 630.
16. K. KISHI, S. UMEBAYASHI and E. TANI, *J. Mater. Sci.* **25** (1990) 2780.
17. L. J. GAUCKLER, J. WEISS, T. Y. TIEN and G. PETZOW, *J. Amer. Ceram. Soc.* **61** (1978) 397.
18. N. E. COTHER and P. HODGSON, *Trans. J. Br. Ceram. Soc.* **81** (1982) 141.
19. E. BUTLER, R. J. LUMBY, A. SZWEDA and M. H. LEWIS, in Proceedings of 1st International Symposium on Ceramic Components for Engines, Japan, 1983, edited by S. Somiya, E. Kanai and K. Ando, (KTK Scientific, Tokyo, 1984) p. 159.
20. M. MITOMO, S. NAGATA and M. TSUTSUMI, *ibid.* p. 311.
21. S. C. SHINGHAL and F. F. LANGE, *J. Amer. Ceram. Soc.* **60** (1977) 190.
22. M. H. LEWIS and P. BARNARD, *J. Mater. Sci.* **15** (1980) 443.
23. Y. HASEGAWA, K. HIROTA, T. YAMANE, M. MITOMO and H. SUZUKI, *Yogyo-kyokai-shi* **89** (1981) 148.
24. H. HASEGAWA, M. MITOMO, K. HIROTA, H. TANAKA, Y. FUJII and H. SUZUKI, *ibid.* **89** (1981) 533.
25. A. K. MUKHOPADHYAY, D. CHAKRABORTY and J. MUKERJI, *J. Mater. Sci. Lett.* **6** (1987) 1198.
26. Y. HASEGAWA, H. TANAKA, M. TSUTSUMI and H. SUZUKI, *Yogyo-kyokai-shi* **88** (1980) 292.
27. C. C.M. WU, K. R. McKINNEY, R. W. RICE, W. J. McDONOUGH and S. W. FREIMAN, *J. Mater. Sci.* **16** (1981) 3099.
28. D. CUBICCIOTTI and K. H. LAU, *J. Amer. Ceram. Soc.* **61** (1978) 512.
29. Y. HASEGAWA, N. YAMANE, K. HIROTA, M. TSUTSUMI and H. SUZUKI, *Yogyo-kyokai-shi* **89** (1981) 46.
30. A. TAKASE, *J. Mater. Sci.* **21** (1986) 329.
31. K. KISHI and S. UMEBAYASHI, *J. Ceram. Soc. Jpn.* **99** (1991) 1250.
32. S. M. WIEDERHORN and N. J. TIGHE, *J. Amer. Ceram. Soc.* **66** (1983) 884.
33. R. K. GOVILA, *J. Mater. Sci.* **23** (1988) 1141.


*Received 20 May*
*and accepted 26 September 1991*